npj | climate and atmospheric science

Article

Published in partnership with CECCR at King Abdulaziz University

Article in Press

https://doi.org/10.1038/s41612-026-01535-0

No evidence of statistically significant Eurasian winter warming or cooling caused by large eruptions over the last millennium

Check for updates

Zilu Meng[1] ✉ & Lorenzo M. Polvani[2,3]

Large tropical volcanic eruptions have been hypothesized to induce surface warming over Eurasia in winter. Recent studies, however, have questioned the robustness of this claim and highlighted the very large internal variability in that season, which can easily overshadow any forced signal caused by such eruptions. To address uncertainties arising from sparse winter proxy data in previous reconstructions, we here examine a recently developed "online" paleo-data assimilation dataset, LMR Seasonal, in which the analysis from one season is propagated forward as the prior for the next season, allowing information from the dense network of summer-sensitive proxies to better constrain winter climate. We examine Eurasian and Northern European temperatures first following the 20 largest tropical eruptions of the last millennium, each exceeding the magnitude of the 1991 Pinatubo event and then, separately, following the largest extra-tropical eruptions over the same period. Irrespective of latitude, we find no evidence of statistically significant wintertime post-eruption warming – or cooling – and correlation analyses show no significant relationship between volcanic stratospheric sulfur injection and subsequent winter temperature anomalies. These findings are corroborated with two additional datasets (WinTEDA and ModE-RA). In addition, analysis of individual eruptions reveals considerable spread across datasets for many events, leading us to question the validity of superposed epoch analysis, which can yield erroneous conclusions even on continental scales.

Large volcanic eruptions are very likely the most important natural forcing of the climate system over the last millennium[1]. In particular, low-latitude eruptions are generally considered the best candidates for producing long-lasting and widespread surface impacts, because sulfur injected into the stratosphere is more likely to enter the upwelling branch of the Brewer-Dobson circulation[2] and form an aerosol cloud that is nearly global in coverage and persists for many months. The direct radiative effects of these aerosols are comparatively well established: they reflect incoming solar radiation and cause surface cooling[3].

Unlike this robust radiatively induced global cooling response, a more controversial circulation-induced surface *warming* response was proposed in the years following the 1991 eruption of Pinatubo[4–6]. Such a warming, limited to Eurasia and to the winter season, would result from a physically plausible mechanism, the so-called "stratospheric pathway"[7,8]. In that mechanism, volcanic aerosols – which are known to absorb upwelling long-wave radiation – cause a warming of the tropical lower stratosphere, resulting in an increased equator-to-pole temperature gradient at those levels, leading to an anomalously strong stratospheric polar vortex in the winter following the eruption[9]. Being dynamically coupled to the troposphere[10], the stronger polar vortex then induces a positive phase of the North Atlantic Oscillation (NAO)[11], which drives milder westerly winds onto Eurasia and produces anomalous surface warming in that region[12]. We stress, however, that this dynamical chain of causality is more uncertain than the direct radiative effects, and remains considerably more difficult to demonstrate. Indeed, the very existence of a post-eruption Eurasian winter warming has been increasingly questioned in recent research.

On the modeling front, the case for a forced Eurasian winter warming has proven challenging. Attempts to validate the original claims, obtained with low-resolution models and highly idealized forcings[7,13], have generally failed to produce a statistically significant winter warming over Eurasia in

[1]Department of Atmospheric and Climate Science, University of Washington, Seattle, WA, USA. [2]Department of Applied Physics and Applied Mathematics, Columbia University, New York, NY, USA. [3]Lamont-Doherty Earth Observatory, Columbia University, Palisades, NY, USA. ✉e-mail: zilumeng@uw.edu

response to even the largest eruptions of the instrumental era, such as the 1991 Mt. Pinatubo eruption [14–17]. An explanation was proposed by recent work showing that the volcanically forced winter response is small compared to internal variability, so that even for Pinatubo (1991) and Krakatau (1883) the observed Eurasian anomalies may largely reflect unforced variability rather than a deterministic response to volcanic aerosols[18,19]. The overwhelming role of internal variability was independently confirmed by a new study[20], which analyzed the historical CMIP6 integrations and reported a forced warming response after Pinatubo (1991) and Krakatau (1883). The warming caused by those eruptions was again found to be much smaller than internal variability, confirming earlier studies; in fact, over 370 model simulations were needed to see the forced response, a number nearly 20 times larger than comparable or larger events that are known to have occurred over the last Millennium.

Searching for larger signals by analyzing simulated eruptions larger than those which occurred after 1850, a Eurasian winter warming in models was reported for the very largest eruptions over the last millennium[21] (typically several times larger than Pinatubo in terms of stratospheric sulfur injection). This modeling result was confirmed by subsequent modeling studies with larger ensembles of simulations[22,23]. We emphasize, however, that even for the very largest events of the Last Millennium the simulated surface warming caused by the eruption is typically smaller than the internal variability of the winter surface temperatures over Eurasia, and thus large ensembles of simulations are needed to establish a statistically significant post-eruption signal[23].

On the observational front, attempts to confirm the early claims[4–6] (which were based on a small number of 19th and 20th century eruptions) have yielded mixed and at times puzzling results. Notably, an analysis[24] of 15 major eruptions since 1500 CE found that the winter warming signal over Europe was surprisingly stronger and more significant in the *second* post-eruption winter, rather than the first, a result that is difficult to reconcile with the proposed stratospheric pathway because the aerosol burden is much smaller by then and the stratosphere has no year-to-year memory.

To explore a bigger set of large eruptions than simply Pinatubo (1991) and Krakatau (1883), a new paleo-data assimilation (PDA) reconstruction of Eurasian *winter* surface temperature (WinTEDA), covering the entire last millennium, was produced and analyzed with a focus on the 20 largest low-latitude volcanic eruptions over that period, all larger than the 1991 Pinatubo eruption: the idea was to seek a possible warming signal by isolating these most powerful events[25]. That analysis revealed that only 7 of the 20 largest events were followed by anomalously warmer surface temperatures, and found no correlation between eruption magnitude and the resulting winter temperatures.

This important null result, however, rests upon a methodology with inherent limitations. WinTEDA is built using an "offline" PDA method[26–28], so that winter temperatures are reconstructed using only winter-sensitive proxies; it also relies on a "static" prior from last millennium simulations to spatially propagate the sparse proxy information. In such a framework, the model provides fixed spatial patterns (covariances) but does not dynamically evolve or produce forecasts, making the reconstruction's quality critically dependent on the density of the proxy network in each season. This dependency is a significant challenge for the last millennium *winter* reconstruction, as winter-sensitive proxies are markedly sparse in the Northern Hemisphere. The vast majority of high-resolution proxies, such as tree rings, reflect summer growing-season conditions[29,30] and are thus not included in WinTEDA. As a result, the proxy network used in that reconstruction consists of fewer than 50 records before 1400 CE, implying a considerable uncertainty in the climate fields of that era.

To overcome those limitations, we here analyze the Last Millennium Reanalysis-Seasonal (LMR Seasonal) reconstruction[31]. Unlike "offline" methods, LMR Seasonal is based on a dynamic "online" data assimilation system[31,32] in which the analysis from one season is propagated forward and used as the prior for the next season. The system integrates a coupled low-order model – a Linear Inverse Model (LIM)[33] – within its assimilation cycle (see the Methods Section for details). This key innovation allows the framework to dynamically propagate climate information from one season (time step) to the next. Consequently, the dense network of summer-sensitive proxies, such as tree rings, can be assimilated to robustly inform the reconstruction of the subsequent autumn and winter, significantly mitigating the data-sparsity problem that affects static reconstructions[31]. This should not be interpreted as a deterministic prediction of the winter circulation from summer conditions; rather, the LMR framework should be understood as using the cross-seasonal covariance and memory in the coupled state vector in order to provide probabilistic constraints on subsequent seasons.

By leveraging this advanced methodology, we here analyze a more reliable reconstruction of Eurasian winter temperatures over the last millennium. We then use this new reconstruction, alongside two independent "offline" PDA datasets (WinTEDA[25] and ModE-RA[34]), to carry out a multi-dataset re-examination of the volcanic winter warming hypothesis. As we will discuss below, our new analysis confirms previous work, and demonstrates that there is no evidence for consistent, forced post-eruption warming – nor of a post-eruption cooling – following the 20 largest events of the last millennium, as any volcanic signal is clearly swamped by internal variability.

Results

LMR seasonal verification

Before analyzing the LMR Seasonal reconstruction to explore post-eruption anomalies, we evaluate it using both instrumental observations and proxy data. As the LMR Seasonal framework incorporates forecasts from the LIM (see the Methods Section), the temperature reconstructions at each time step are not independent, because they combine the current seasonal prior with information propagated from earlier seasons. This feature is particularly important for our December-January-February (DJF) work, when proxy coverage is severely limited. As shown in a prior study[31], LMR Seasonal achieves higher DJF temperature correlation skill than other methods, even while using fewer proxies. Focusing on Eurasia, our validation here consists of two steps.

First, for instrumental validation, we compare LMR reconstructed 2-meter air temperatures in DJF with the HadCRUT5 dataset[35]. The correlation map between the reconstructed winter temperatures and HadCRUT5 over the period 1880–2000 CE is shown in Fig. 1a. Correlations exceed 0.4 across most of Eurasia and are particularly high in Northern Europe (greater than 0.7), indicating that a reconstruction obtained using proxy assimilation alone still aligns well with instrumental observations.

Second, as instrumental data are limited to the past ~150 years, we extend the validation by comparing LMR against withheld proxy records that are excluded from the assimilation in each bootstrap iteration, following the approach of a prior study[27]. We use the PAGES2k V2 dataset[30], withholding a subset of proxies during assimilation using a bootstrap procedure. We randomly withhold 20% of the proxies and repeat the DA procedure over 50 bootstrap iterations. In each iteration, the reconstructed temperatures are forward-modeled into proxy space using the Proxy System Model (as illustrated in the Methods Section), allowing for direct comparison with the withheld proxy records. Validation performance is quantified by the temporal correlation between the reconstructed and observed proxy time series. As shown in Figure 1b, the 50-iteration mean correlations are high across Northern Europe (mostly above 0.8) and are positive across most of Eurasia, indicating strong agreement between the reconstruction and these withheld proxy records over the last millennium. These results confirm the reliability of the LMR reconstruction for assessing Eurasian winter temperatures.

Post-eruption Eurasian temperature anomalies

Having validated the LMR Seasonal reconstruction, we now turn to exploring winter temperature anomalies over Eurasia, and potential volcanic impacts in that region and season. For consistency with earlier studies[18,19,23], we define anomalies as the difference between a given winter and the average of the preceding five winters, and characterize Eurasia with a

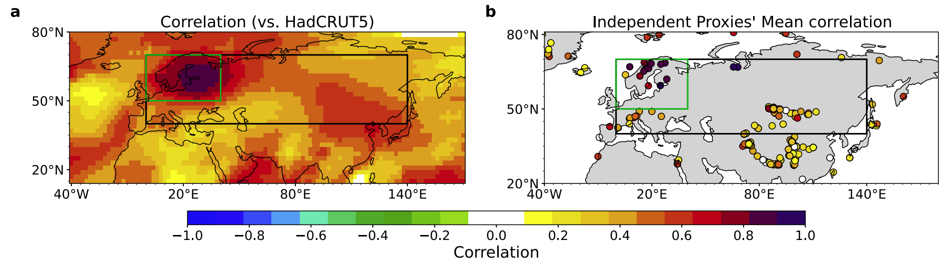

Fig. 1 | Validation of LMR Seasonal winter temperatures. **a** shows the temporal correlation between LMR Seasonal reconstructed winter temperatures and HadCRUT5 over 1880–2000 at each grid point. **b** shows the mean temporal correlation between withheld proxy records, excluded from each assimilation iteration, and reconstructed winter temperatures over 850–2000. Each circle in (**b**) denotes a proxy site, and the circle color denotes the strength of the correlation. The black rectangles mark the Eurasian analysis domain, and the green rectangles mark the Northern European analysis domain. LMR stands for Last Millennium Reanalysis, and HadCRUT5 is the instrumental surface temperature dataset used for verification.

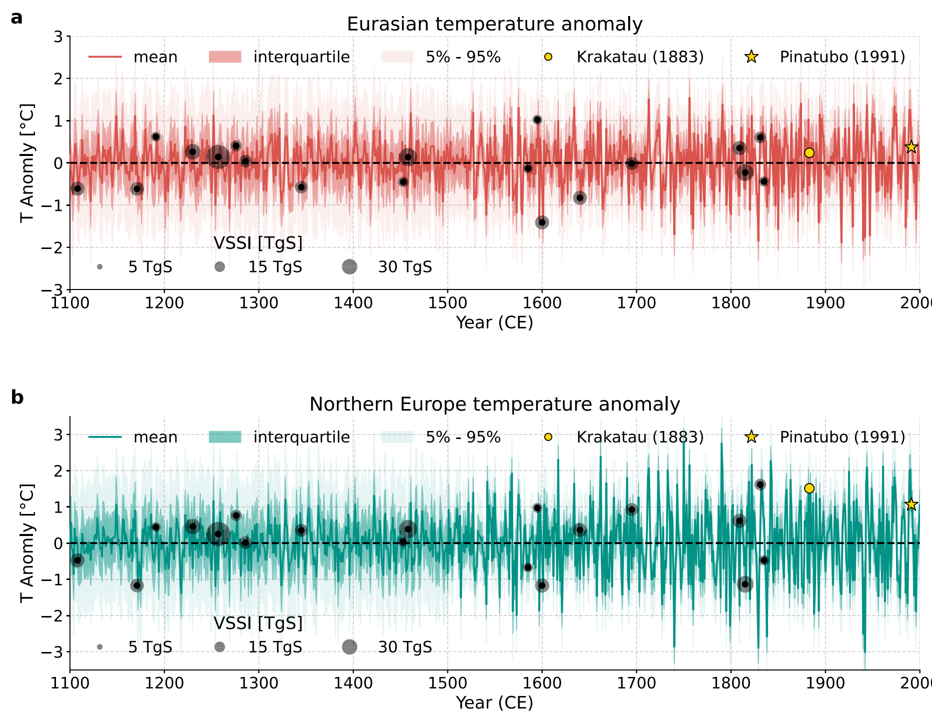

Fig. 2 | Eurasian and Northern European winter temperature anomalies in the context of volcanic forcing. **a** shows the December–January–February (DJF) temperature anomaly time series over Eurasia reconstructed with LMR Seasonal, and **b** shows the corresponding series over Northern Europe. The solid line denotes the ensemble mean, the dark shaded region denotes the interquartile range, and the light shaded region denotes the 5–95% interval. Dark gray circles identify the first winter after the major tropical volcanic eruptions considered here, with circle size scaled by volcanic stratospheric sulfur injection (VSSI; 5, 15, and 30 TgS). The yellow circle and yellow star highlight the 1883 Krakatau and 1991 Pinatubo eruptions, respectively. DJF denotes boreal winter, and TgS denotes teragrams of sulfur.

simple latitude-longitude box (see Methods, and the black box Fig. 1). Before discussing eruptions, it is instructive to consider the entire time-series of Eurasian winter temperature anomalies, shown by the red line in Fig. 2a. While the ensemble mean value is typically confined between ±1 °C, the 5%–95% confidence extends to ±2 °C, with many individual winters experiencing anomalies in excess of ±2 °C. The point we wish to highlight here is that internal variability is considerable over Eurasia in winter, and any anomaly caused by an external forcing needs to be placed in that context.

With this in mind, we now proceed to examine the anomalies following all the large, low-latitude eruptions of the last millennium. For consistency with an earlier study[see their Table 1][25], we focus here on the 20 eruptions whose volcanic stratospheric sulfur injection (VSSI) is greater than that of the 1991 Pinatubo eruption (~9 TgS); the full list is given in Table S1. The largest event, Samalas (1257), resulted in a VSSI of ~60 TgS (about 7 times larger than Pinatubo), followed by an unnamed eruption in 1458 with a VSSI of ~33 TgS, and by the Tambora 1815 eruption (VSSI ~28 TgS), with the other eruptions in the 10–20 TgS range. We emphasize that all of the events analyzed here are larger (in VSSI) than those analyzed in the original paper[5], suggesting a post-eruption warming, which only included a dozen events. Given the larger size of our set of historical events, and their much larger VSSI, one would expect a forced signal in the post-eruption winters to appear. Alas, no consistent sign in the post-eruption winter temperature emerges, as seen in the gray dots in Fig. 2a (the size of the dots indicates the VSSI). Nearly all post-eruption anomalies are found well within the range of Eurasian winter variability (roughly ±1 °C), and many non-eruption winters exhibit anomalies of comparable or larger magnitude. Thus, post-eruption winters are unremarkable in the full millennium record. This is also true for Krakatau (1883) and Pinatubo (1991), which are highlighted in yellow in Fig. 2a: their first post-eruption winters fall well within the broader range of winter variability.

It could be argued, with good reason, that given the relative paucity of proxies over Siberia, the absence of a consistent post-eruption signal might simply be a consequence of the absence of observations. To address this objection we decided to examine a smaller area, centered over Northern Europe (see the green boxes in Fig. 1): since Northern Europe benefits from high-quality tree-ring proxies and documentary temperature records[36], and since that region is immediately adjacent to the North Atlantic and thus directly affected by anomalies in the NAO (possibly caused by stratospheric anomalies accompanying volcanic eruptions), it is the prime location to detect a volcanic warming signal, as noted in an earlier observational study[24]. In addition, this region exhibits particularly high verification skill in

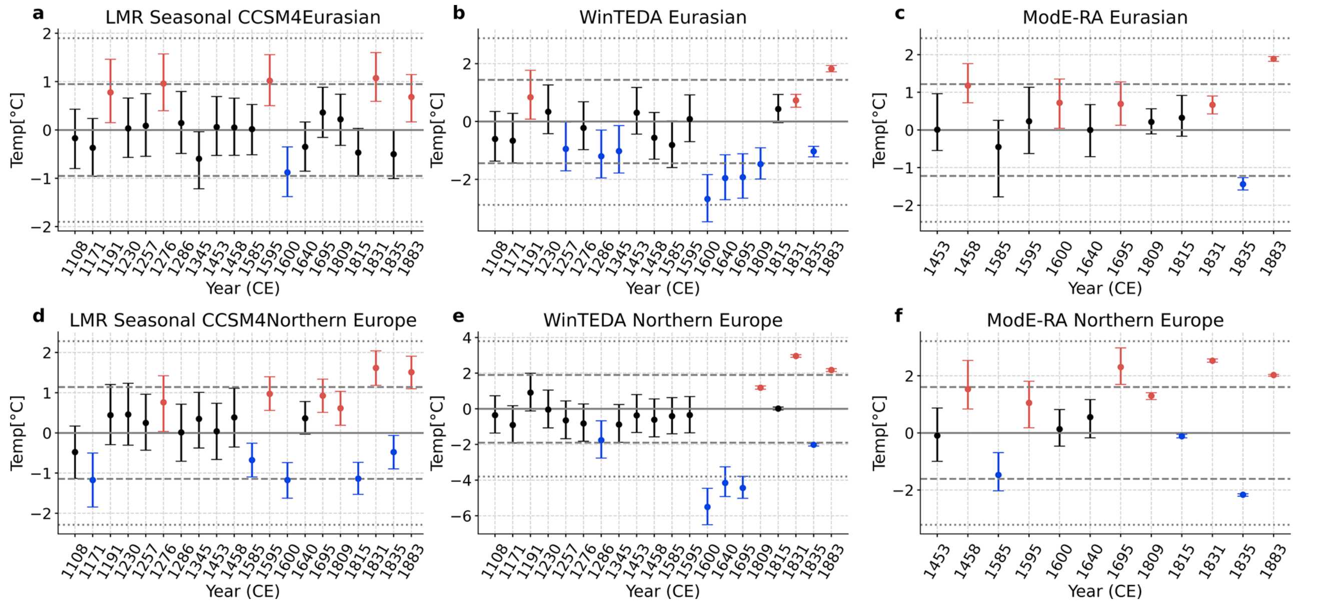

Fig. 3 | Post-eruption winter temperature anomalies across three paleo-data assimilation reconstructions. The panels show the first post-eruption DJF temperature anomalies over Eurasia (top row) and Northern Europe (bottom row) in the LMR Seasonal (left column), WinTEDA (middle column), and ModE-RA (right column) reconstructions. Each event is shown by a dot, and the corresponding bar shows the mean and the 25th–75th percentile interval. Red bars denote significant warming, defined by a 25th percentile above zero; blue bars denote significant cooling, defined by a 75th percentile below zero; and black bars denote non-significant anomalies. The horizontal solid gray line denotes zero anomaly, the gray dashed lines denote the ±1 standard deviation range, and the gray dotted lines denote the ±2 standard deviation range. PDA stands for paleo-data assimilation, and DJF denotes December–January–February.

Figure 1, giving us greater confidence in the reconstruction there. Alas, over that region too (see Fig. 2b), our new reconstruction reveals that post-eruption winters over Northern Europe do not stand out from the internal variability. It is tantalizing to observe that, over this smaller region, 14 of 20 events showed post-eruption warming, but that fact alone is not sufficient to establish the existence of a robust forced response, because the majority of those anomalies are not statistically significant and remain comparable in magnitude to ordinary winter variability, as we discuss next.

To illustrate the statistical significance and summarize the findings from the LMR Seasonal reconstruction, we show the first post-eruption winter temperature anomaly for each of the 20 events of interest in Fig. 3a and d, over Eurasia and over Northern Europe, respectively. Red and blue bars indicate statistically significant warming and cooling, respectively, defined as cases where the reconstructed 25th/75th percentile is above/below zero; black bars denote non-significant anomalies. Over Eurasia, the LMR reveals that only 3 of 20 eruptions are followed by significant winter warming, 5 are followed by cooling, and the remaining 12 by insignificant anomalies (panel a). Over Northern Europe, with the much denser proxy network, these numbers are qualitatively similar: 6 of 20 are followed by significant warming, 5 by significant cooling, and the remaining 9 by insignificant anomalies. We therefore conclude that the LMR Seasonal reconstruction provides no evidence of a consistent post-eruption Eurasian winter warming – or cooling – once the large background winter variability is taken into account. It is not impossible that a winter warming caused by a large eruption might exist, but there is no evidence for it in the LMR temperature reconstruction.

This null result confirms the findings of an earlier study[25] which analyzed the same 20 large eruptions but using the static WinTEDA reconstruction, based solely on the much sparser winter-sensitive proxies. For direct comparison, the WinTEDA post-eruption winter anomalies are shown in Figures 3b and e, for the two regions of interest. In addition, we have also examined the anomalies in a third recent reconstruction, ModE-RA[34], and these are shown in Fig. 3c and f. As this dataset only extends back to 1421, only the most recent 12 eruptions are available. Of those, 5 show significant warming, while the remainder show cooling or insignificant anomalies. Beyond the lack of a consistent warming or cooling signal, and the fact that for several events the three reconstructions we have analyzed disagree on the sign of the anomalies, an important take-home message from Fig. 3 is post-eruption winter anomalies are within two standard deviations of the mean for each reconstruction (shown in the thin dotted lines), for nearly all events, indicating that internal variability overwhelms any potential effect of volcanic forcing.

The overwhelming role of internal variability is also clearly seen in Fig. 4, where we explore whether larger eruptions are associated with larger winter temperature anomalies (as one might expect). In all three reconstructions, the correlations with VSSI are weak and statistically insignificant. In LMR Seasonal, for example, the correlations are $r = -0.06$ ($p = 0.81$) for Eurasia and $r = -0.14$ ($p = 0.55$) for Northern Europe, and these conclusions are unchanged when the 1257 Samalas eruption is excluded from the analysis (Fig. S1). Similar results are found in the other two datasets, confirming the lack of evidence linking eruption magnitude directly to regional temperature responses. ModE-RA shows the strongest correlation (Fig. 4c): over Eurasia we find a statistically insignificant 0.31 value (i.e., with the eruption magnitude accounting for less than 10% of the spread across the 12 events) which, surprisingly, gets even weaker over Northern Europe (Fig. 4f) where most of the proxies are found. Thus, eruption magnitude explains little of the inter-event spread in post-eruption winter anomalies.

One might wonder to what degree our LMR Seasonal results are sensitive to the model prior used. Recalling that WinTEDA and ModE-RA each employ different climate models as priors for their static assimilation procedure, CESM and MPI, respectively, we have produced two additional LMR Seasonal reconstructions using those two models to train the LIM model, which serves as the dynamical prior in LMR (i.e., we replaced CCSM4, the standard LMR model, with CESM and MPI; see Methods). As one can see in Figs. S2 and S3, these additional dynamic LMR datasets likewise yield null results, both for individual events and for the regression with VSSI, thereby reinforcing the robustness of our findings.

At this point, it is highly informative to revisit the so-called "superposed epoch analysis" (SEA) method, which is still widely used in studies examining the influence of volcanic eruptions on climate[24,37]. This technique, which amounts to averaging all available events – irrespective of their magnitude – is prone to yielding non-robust results, and has been previously

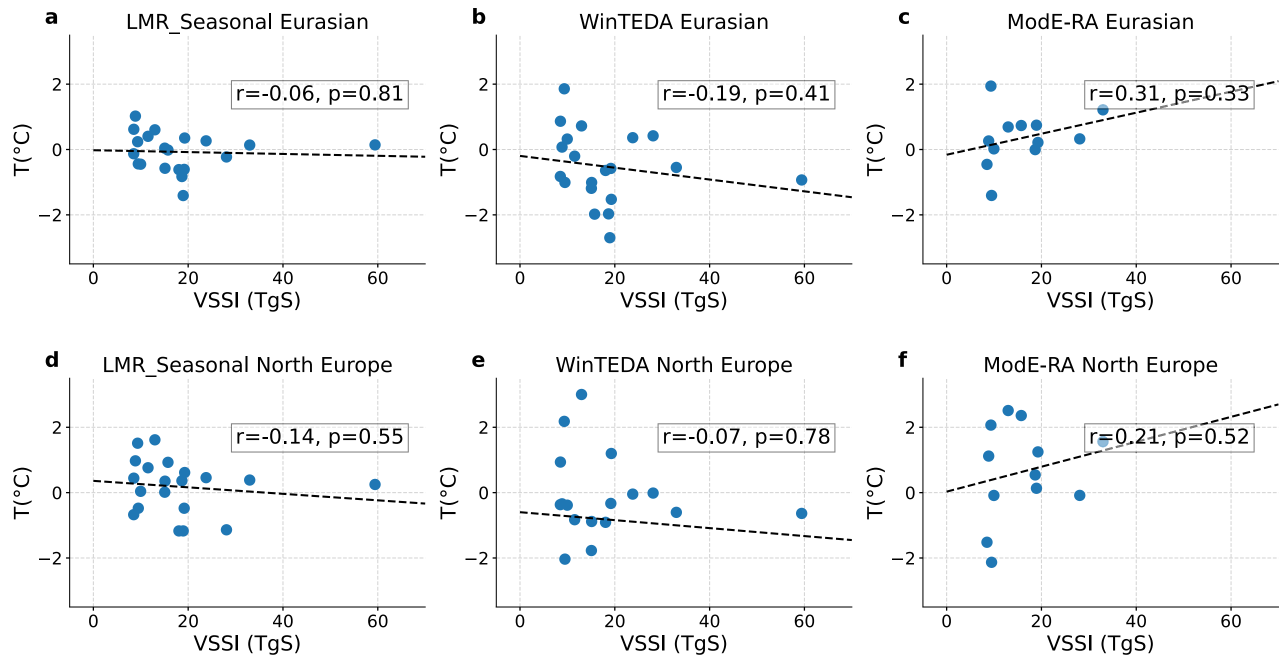

Fig. 4 | Relationship between eruption magnitude and post-eruption winter temperature anomalies. The scatter plots show volcanic stratospheric sulfur injection (VSSI; TgS) against the reconstructed temperature anomaly in the first post-eruption DJF winter for LMR Seasonal (left column), WinTEDA (middle column), and ModE-RA (right column), over Eurasia (top row) and Northern Europe (bottom row). Each point denotes one eruption, and the black dashed line denotes the least-squares linear fit. The correlation coefficient (*r*) and *p*-value (*p*) are reported in each panel. Across all panels, the correlations are weak and not statistically significant. DJF denotes December–January–February, and TgS denotes teragrams of sulfur.

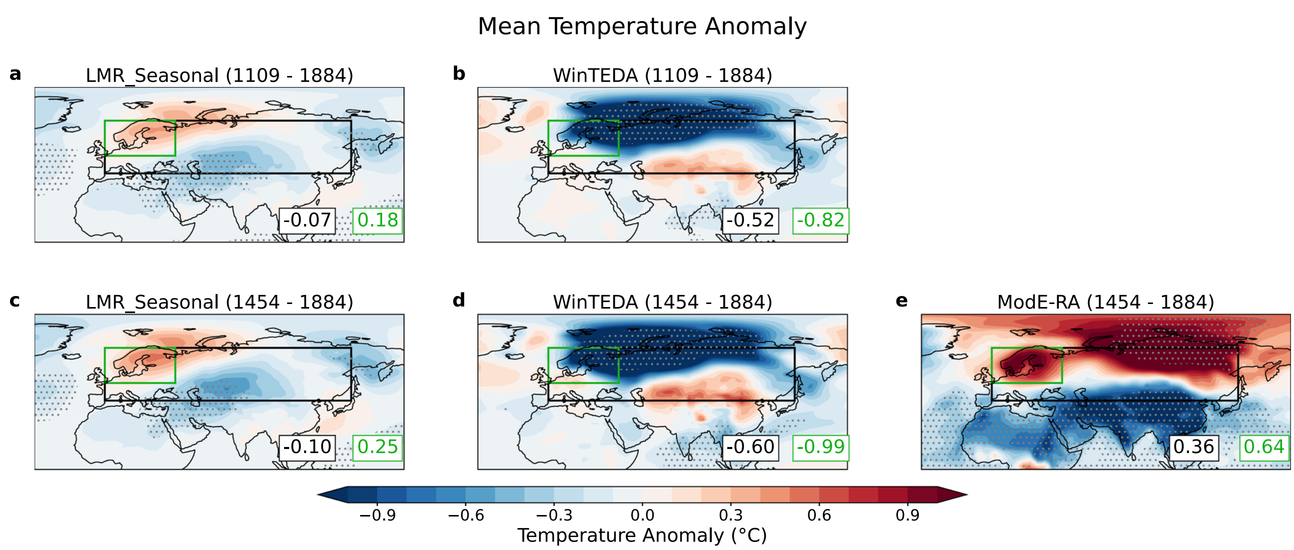

Fig. 5 | Superposed epoch analysis of post-eruption surface temperature anomalies across three reconstructions. The top row shows the composite DJF temperature anomaly averaged over the 20 largest tropical eruptions of the last millennium, and the bottom row shows the same analysis for the 12 eruptions common to all three reconstructions after 1454. Columns correspond to LMR Seasonal, WinTEDA, and ModE-RA. Stippling denotes values significant at the 95% level. The black rectangles mark the Eurasian domain, and the green rectangle marks the Northern European domain. The numbers in the black and green boxes give the domain-averaged, event-averaged anomalies over Eurasia and Northern Europe, respectively. DJF denotes December–January–February.

critiqued[38]. In particular, when the signal being sought is small compared to internal variability, the SEA is primarily shaped by that variability, rather than by the small signal being sought. Furthermore, since the climate response of an eruption is expected to be larger for larger VSSI, the SEA method dilutes volcanic impacts that might accompany the larger eruptions by averaging them with the smaller ones whose signal is likely undetectable. To illustrate this, we show the SEAs for all 20 events in LMR and WinTEDA in the top row of Fig. 5 and, in the bottom row, for the smaller set of 12 post-1421 events for all three reconstructions (LMR, WinTEDA and ModE-RA). Notice the considerable lack of agreement across these SEAs: LMR Seasonal indicates non-significant warming in Northern Europe and weak cooling elsewhere, while WinTEDA indicates strong and significant cooling nearly everywhere, and ModE-RA suggests non-significant warming over Northern Europe but significant warming over Siberia.

What is one to make of these contradictory results? Our suggestion is that the SEA does not actually represent anomalies caused by volcanic eruptions. To appreciate this, we invite the reader to examine each eruption *individually*: all 20 events are shown in Figs. S4–S7. Consider first the five eruptions in the 19th century (shown in Fig. S4), and note that for these events there is good agreement between the reconstructions over Northern Europe, where the largest concentration of proxies is found. Two events show post-eruption cooling (1835 and 1815) and three show post-eruption warming (1883, 1831, 1809): most importantly, all three datasets concur on the sign of the anomalies after each eruption. However, over the larger Eurasian area, especially Siberia, where the proxies are sparser, the agreement is not as good, even for these relatively recent eruptions. As one goes further back in time, some stark disagreements appear across reconstructions. For example, consider the 1600 Huaynaputina event, whose VSSI is roughly twice the one of Pinatubo (1991), and which exhibits the largest post-eruption cooling in both LMR and WinTEDA (as seen in Figure 3a, b, d, e): in both of those reconstructions the cooling is widespread, from Europe all the way to Eastern Siberia (Fig. S5g, h), and yet ModE-RA shows an equally large *warming* over most of Eurasia (Figure S5). The inevitable conclusion is that, on the basis of these three reconstructions, we are at present unable to determine *even the sign* of the post-eruption anomalies for that event. And, finally, let us consider the 1257 Samalas eruption (Figures S7a,b), keeping in mind that it is the eruption with the largest VSSI of the last 6000 years[39]: even for that massive event, LMR and WinTEDA fail to agree on the sign of the post-eruption anomalies in winter.

Discussion

The one robust conclusion that emerges from our analysis of the LMR Seasonal reconstruction is that – at this time – there is no observational evidence of a signal on surface temperature over Eurasia caused by large tropical eruptions, be it a warming or a cooling. This confirms recent studies[25,40], and questions the early claims[4–6,24] of post-eruption winter warming. More troubling still is the considerable disagreement among state-of-the-art temperature reconstructions, of which we have highlighted some egregious examples above. While the reader can find several cases of agreement among the reconstructions (Figs. S4–S7), when considering that the events analyzed are the very largest eruptions across the Last Millennium, the degree of disagreement is concerning.

Considering all 20 largest events together (see Fig. S8), we find that over Northern Europe LMR Seasonal shows a stronger correlation with ModE-RA ($R = 0.79$) than with WinTEDA ($R = 0.49$), whereas over the broader Eurasian domain LMR Seasonal correlates more strongly with WinTEDA ($R = 0.58$) than with ModE-RA ($R = 0.22$). We believe these discrepancies are primarily due to methodological differences. Key among these are (1) the use of state-dependent, evolving prior covariances in LMR Seasonal versus the static priors used in ModE-RA and WinTEDA, and (2) the dynamic, cross-seasonal propagation of information (e.g., from the data-rich summer to the data-sparse winter) in our "online" framework. Crucially, despite these distinct methodological approaches and clear disagreement on some individual events, all three datasets concur to support our primary conclusion: the absence of a consistent, forced winter temperature response over Eurasia. This consistency across different reconstruction techniques significantly strengthens the robustness of our finding.

The only remaining evidence of a post-eruption warming, at present, comes from model simulations[20,22,23]. Whether this warming is a modeling artifact or a realistic feature remains an open question, but we emphasize that the forced warming seen in models is relatively small and hard to detect. First, a VSSI larger than 20 TgS is required to produce a statistically significant warming in models (implying no detectable signal from Pinatubo 1991, Krakatau 1883, and similarly sized events). Second, large ensembles of simulations are needed to establish statistical significance in models, and the ensemble sizes needed to achieve significance are in excess of the number of known eruptions over the Last Millennium. Third, in model simulations the post-eruption Eurasian warming is never larger than the internal variability, and hence unlikely to cause catastrophic conditions[23]. In addition, modes of coupled variability such as ENSO may further modulate the winter response from one eruption to the next, thereby increasing event-to-event spread and complicating detection of any stable Eurasian signal[41].

Table 1 | Northern Hemisphere volcanic eruptions greater than 2 TgS in VSSI from the eVolv2k_v3 database[46]

Year	VSSI (TgS)	σ VSSI (TgS)	Month	Day
1182	10.05	2.98	–	–
1210	3.29	1.26	–	–
1453	9.97	3.07	–	–
1510	2.30	0.83	7	25
1567	2.51	0.82	–	–
1667	3.48	1.11	9	23
1729	4.82	1.49	–	–
1739	3.44	1.09	8	19

The unknown month and day of the eruption is indicated as "–". The σ indicates the uncertainty.

We conclude by examining the question of low-latitude versus high-latitude eruptions. It is widely believed that low-latitude eruptions are the best candidates for causing long-lasting and widespread surface impacts, as stratospheric sulfur injections into the upwelling branch of the Brewer-Dobson circulation are most likely to produce an aerosol cloud that is nearly global in coverage and lasting many months. However, two recent studies[42,43] have argued that extra-tropical eruptions in the Northern Hemisphere (NH) might have a disproportionately strong annual-mean cooling effect on that hemisphere, as large as 3 to 7.5 times that of tropical eruptions per unit of sulfur injected, owing to the hemispheric confinement of the aerosol cloud, whose impact is then amplified by yet undetermined mechanisms.

It is natural, therefore, to examine Northern Hemisphere extra-tropical eruptions over the last millennium with regard to a potential winter warming over Northern Europe and Eurasia. To do so, we select all NH extra-tropical eruptions with VSSI values greater than 2 TgS in the Last Millennium (see Methods): these 8 events are listed in Table 1. Their post-eruption temperature anomalies are, as one might expect, as unimpressive as those following the low-latitude events. As seen in Figs. 6a and d, LMR Seasonal shows that two events are followed by significant warming, two by significant cooling, and four by insignificant anomalies, over both Eurasia and Northern Europe. The other two "static" reconstructions confirm the lack of a consistent post-eruption winter signal, warming or cooling, for these largest extra-tropical events.

The alert reader will have noticed that the Laki eruption of 1783 was not included in Table 1: we excluded it to offer a clean comparison to an earlier paper that also excluded it[43]. However, a new modeling study has argued that volcanic aerosols from the 1783 Laki eruption produced a winter warming over Northern Eurasia, even while conceding that the temperature anomaly after the eruption was "not statistically significant in the traditional sense"[44]. Without going into the merits of the modeling component of that study, we simply note here that our multi-reconstruction analysis provides no evidence of surface impacts caused by Laki. Averaging over the same Eurasian domain used in that study (55–70°N, 30–150°E), we present the time series of surface temperature anomalies for our three reconstructions, for direct comparison with their Figure 2. Among the three reconstructions, only ModE-RA shows a pronounced DJF 1784 warming anomaly of approximately 1.5°C, whereas LMR Seasonal and WinTEDA show much weaker warming anomalies of approximately 0.5°C (Fig. 7). Moreover, the time series in Figure 7 indicates that the DJF 1784 anomaly lies well within the range of winter internal variability, implying that this single warm winter cannot by itself be uniquely attributed to volcanic forcing. Notice how the winter of 1783–84 is in no way exceptional, as many winters in the two decades 1776–1796 show comparable warm anomalies and yet are not preceded by an eruption.

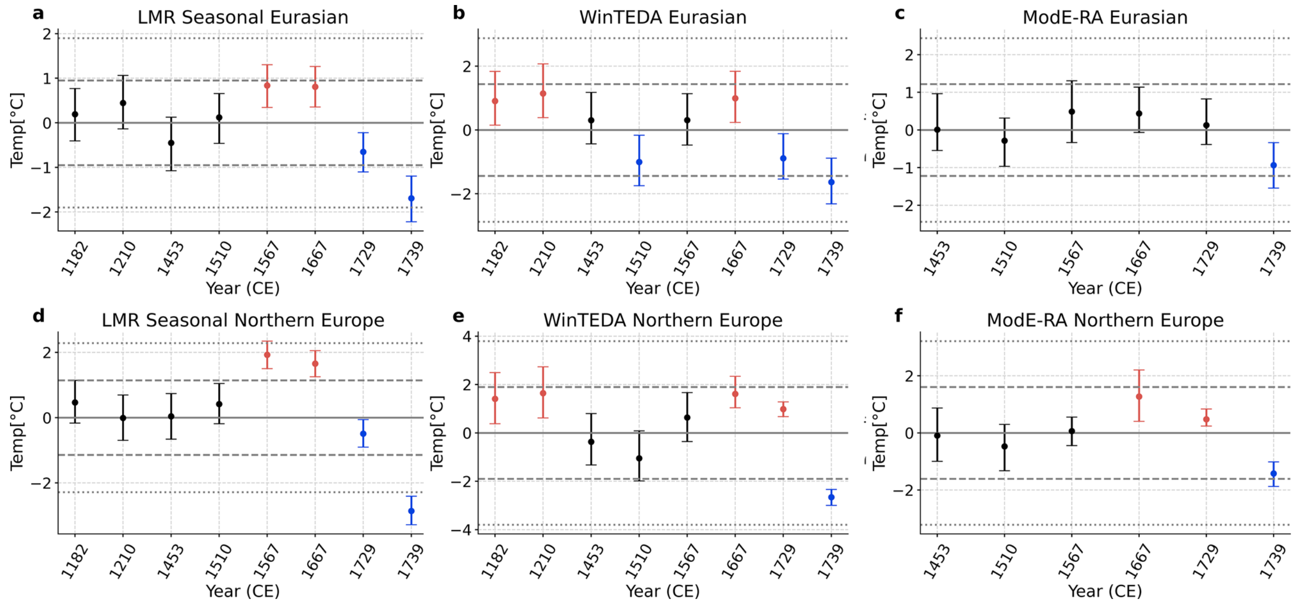

Fig. 6 | Winter temperature anomalies following the eight largest Northern Hemisphere extra-tropical eruptions across three reconstructions. The panels show post-eruption DJF temperature anomalies over Eurasia (top row) and Northern Europe (bottom row) in the LMR Seasonal (left column), WinTEDA (middle column), and ModE-RA (right column) reconstructions, following the eight extra-tropical eruptions listed in Table 1. Red bars denote significant warming, blue bars denote significant cooling, and black bars denote non-significant anomalies, using the same percentile criteria as in Fig. 3. The horizontal solid gray line denotes zero anomaly, the gray dashed lines denote the ±1 standard deviation range, and the gray dotted lines denote the ±2 standard deviation range. DJF denotes December–January–February.

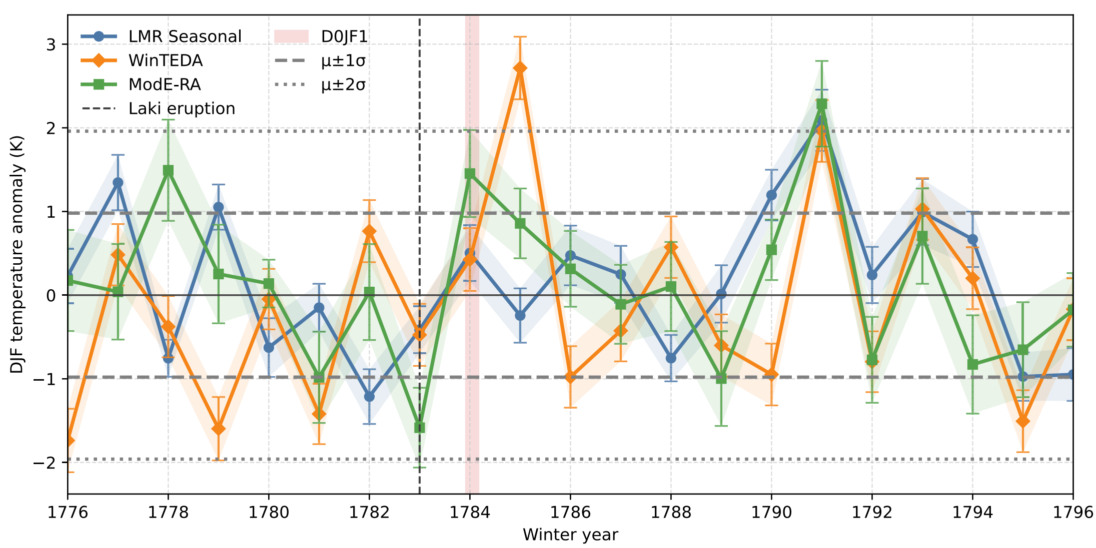

Fig. 7 | DJF temperature anomalies over Northern Eurasia following the 1783 Laki eruption. The figure compares December–January–February (DJF) temperature anomalies over Northern Eurasia (55–70°N, 30–150°E) in LMR Seasonal, WinTEDA, and ModE-RA. Anomalies are defined relative to the mean of the previous five winters (years $N-5$ to $N-1$), based on the ensemble mean. The winter year corresponds to the January–February year, so 1784 denotes December 1783 to February 1784. Solid lines denote ensemble means; shaded bands and error bars denote two-sided 90% confidence intervals; the vertical dashed line marks the eruption timing, and the red shaded band marks the first post-eruption winter. The horizontal solid gray line denotes zero anomaly, the gray dashed lines denote the ±1 standard deviation range, and the gray dotted lines denote the ±2 standard deviation range.

Furthermore, the spatial pattern of the reconstructed DJF 1784 anomalies (shown in Fig. S9) cannot be reconciled with the proposed dynamical interpretation. If the warming were primarily mediated by a positive NAO phase, one would expect the strongest warming to be over Northern Europe, where the influence of North Atlantic circulation anomalies is strongest. Instead, all three reconstructions show a robust *cooling* over Europe in DJF 1784, whereas the regions of warming over Asia disagree among the reconstructions. Note how ModE-RA and WinTEDA show nearly opposite anomaly patterns, and LMR Seasonal is quite different as well. In other words, it remains unknown at present which Asian regions actually experienced any warming after the 1783 Laki eruption. Thus, the available reconstructions provide little evidence to support any Eurasian winter warming caused by that event.

In conclusion, our multi-dataset, event-level analysis confirms that internal climate variability overwhelmingly shapes Eurasian winter temperature anomalies. Using state-of-the-art reconstructions and methods, we are unable to detect a consistent and significant influence of tropical (or extra-tropical) explosive volcanism on winter Eurasian temperatures.

Methods

Seasonal Paleo Data Assimilation (PDA)

Our analysis is based on Last Millennium Reanalysis–Seasonal (LMR Seasonal) surface temperatures[31], which are obtained using a dynamic, online paleo-data assimilation framework designed to reconstruct seasonal climate over the last millennium. As illustrated in Fig. 8a, the LMR Seasonal framework operates as a cycling seasonal assimilation system. The state vector $\mathbf{x}$, which comprises the leading principal components of five key climate variables (2-meter air temperature, sea surface temperature, upper-ocean heat content, and Northern Hemisphere (NH) sea-ice concentration and thickness), evolves forward in time according to a linear inverse model, expressed as $d\mathbf{x}/dt = \mathbf{L}\mathbf{x} + \boldsymbol{\xi}$, which produces a prior estimate of the climate state for a given season, $\mathbf{x}_p$. That prior is mapped into proxy space through a proxy system model to produce an expected proxy estimate, $\mathbf{y}_e = \mathcal{H}(\mathbf{x}_p)$, which is then compared with the actual proxy observations, $\mathbf{y}$. The resulting innovation, $\mathbf{y} - \mathbf{y}_e$, is assimilated with an Ensemble Kalman Filter to obtain the analysis state, $\mathbf{x}_a$, and that updated state is then propagated forward to the next season.

Figure 8 b shows why the LMR Seasonal online assimilation cycle is especially useful for winter reconstruction: proxy availability is strongly season-dependent, with far more records in JJA than in DJF. By carrying information forward across MAM, JJA, SON, and DJF, the framework allows the dense network of summer-sensitive proxies to inform the subsequent autumn and winter reconstruction, thereby alleviating the severe sparsity of winter-sensitive proxy records. A full description[31] of the LMR framework is available in the literature, so we here only summarize the elements most relevant to the present study.

The dynamical core of LMR Seasonal is a Linear Inverse Model (LIM), trained on last-millennium climate model simulations, which provides seasonal forecasts of the evolving climate state[31,32]. The LIM is applied to a reduced state vector that includes the leading large-scale modes of near-surface air temperature, sea surface temperature, upper-ocean heat content, and Northern Hemisphere sea ice. In the present study, its most important role is to propagate information from one season to the next within the assimilation cycle, which is the key feature enabling summer-sensitive proxies to constrain winter conditions. Our standard reconstruction uses a LIM trained on CCSM4 last-millennium simulations, and we additionally test the sensitivity of the results using LIMs trained on CESM and MPI simulations.

Proxy observations are linked to the climate state through proxy system models (PSMs), which map model temperature fields into proxy space. We assimilate 521 temperature-sensitive proxy records from the PAGES2k V2 database[30], including tree rings, corals, and ice cores. Each proxy is assigned an objectively determined seasonal sensitivity following the calibration procedure[for further details][28,31]. This seasonally resolved proxy treatment, applied to proxy records with explicitly assigned seasonal sensitivity (primarily summer-sensitive tree-ring records), is crucial for the online framework, because it permits summer-sensitive records to influence later seasons through the model dynamics.

The assimilation is performed with an 800-member Ensemble Kalman Filter (EnKF)[45]. At each seasonal step, the EnKF updates the LIM prior using the proxy observations available for that season, and the updated analysis then provides the initial condition for the forecast into the next season. This sequential, online updating distinguishes LMR Seasonal from static, offline PDA products, because the analysis from each season becomes the initial condition for the forecast into the next season. As a result, information from proxy-rich seasons, especially summer, can be dynamically carried forward

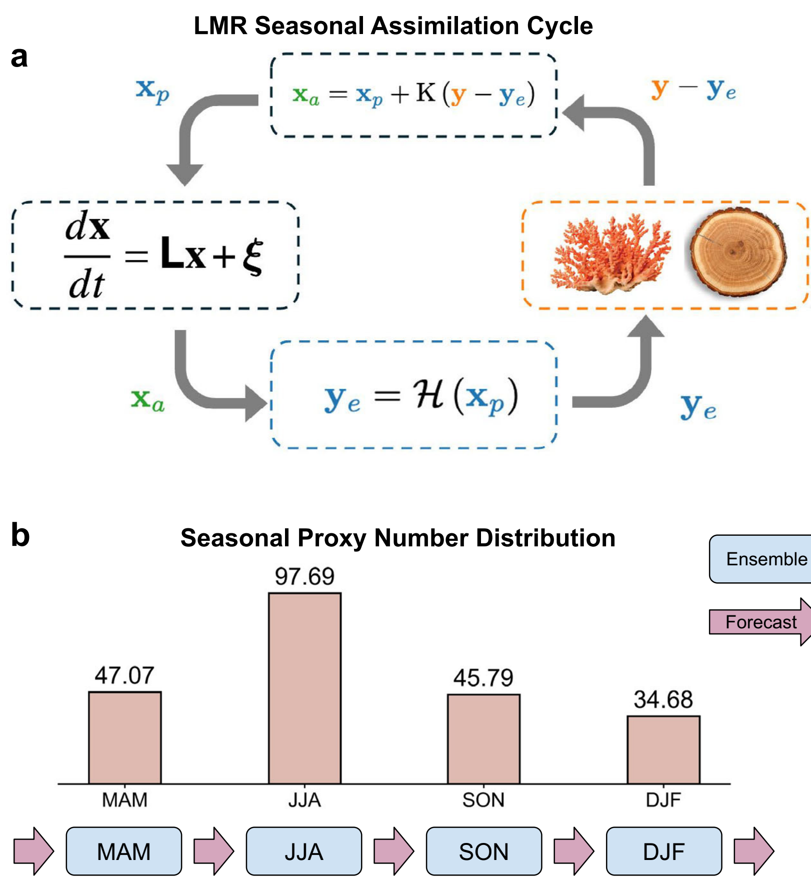

Fig. 8 | Schematic illustration of the LMR Seasonal framework. **a** summarizes the LMR Seasonal assimilation cycle. The dynamical model produces a prior state ($\mathbf{x}_p$), the proxy system model maps that state into proxy space ($\mathbf{y}_e = \mathcal{H}(\mathbf{x}_p)$), and the innovation ($\mathbf{y} - \mathbf{y}_e$) is assimilated using the Ensemble Kalman Filter with Kalman gain $\mathbf{K}$ to produce the analysis state ($\mathbf{x}_a$). The analysis state is then propagated forward to the next season with the linear inverse model, written as $d\mathbf{x}/dt = \mathbf{L}\mathbf{x} + \boldsymbol{\xi}$, where $\mathbf{L}$ is the linear dynamical operator, and $\boldsymbol{\xi}$ is the stochastic forcing term. **b** shows the mean number of available proxy records by season in the PAGES2k V2 database, together with the sequential progression from March–May (MAM) to June–August (JJA) to September–November (SON) to December–February (DJF). The strong seasonal maximum in JJA and the minimum in DJF illustrate why cross-seasonal propagation is important for winter reconstruction. LMR stands for Last Millennium Reanalysis, and MAM, JJA, SON, and DJF denote the four seasonal windows used in the cycling framework.

into autumn and winter, whereas offline PDA products rely on fixed prior covariances and do not explicitly propagate information through the seasonal cycle.

In summary, LMR Seasonal is a fully coupled, online seasonal data assimilation framework in which a dynamical prior, proxy forward models, and ensemble-based updates are combined within a cycling system. For the purposes of this study, its main advantage is that it provides a more robust winter reconstruction over Eurasia by dynamically propagating information across seasons.

Additional PDA datasets for corroboration

To ensure the robustness of our findings, we analyze two additional PDA datasets: ModE-RA[34] and WinTEDA[25]. Both employ an "offline" assimilation approach, which differs fundamentally from our "online" LMR Seasonal framework. In an offline system, the EnKF updates a "static" prior from a climate model simulation without a dynamic forecast step. Consequently, their winter reconstructions are constrained exclusively by the sparse network of winter-sensitive proxies (e.g., specific ice cores and Southern Hemisphere tree rings), particularly before the instrumental era. However, a key advantage of ModE-RA and WinTEDA is their assimilation of instrumental temperature observations. This significantly enhances the skill of their reconstructions during the more recent period (post-1800), especially over data-rich regions like Northern Europe. By including these independent, offline datasets in our analysis, we aim to robustly validate our conclusions across different methodological approaches.

Last millennium volcanic data

Abundant modeling evidence[15,18,22,23] suggests that eruptions comparable to Pinatubo (1991) are insufficiently strong to produce such a significant winter surface response over Eurasia. Therefore, following a previous study[25], we here focus on low-latitude eruptions over the last millennium (LM) that exceed the magnitude of Pinatubo. We use the eVolv2k_v3 volcanic forcing database[42,46], based on ice core records from Greenland and Antarctica, which provides estimates of eruption latitude and volcanic stratospheric sulfur injection (VSSI) from 500 BCE to 1900 CE. From this dataset, we identify 20 low-latitude eruptions between 1000–1900 CE with VSSI values greater than Pinatubo (8.78 Tg S); their dates can be seen on the *x*-axis of Fig. 3. Given recent interest, we also examine a set of 8 major Northern Hemisphere (NH) extratropical eruptions.

Analysis methods

As discussed in previous studies[18,25] and reviewed in the introduction, we focus on the first DJF winter following each eruption, as the stratosphere lacks sufficient memory to maintain a volcanic influence beyond the initial post-eruption season. Following our original study[18], surface temperature anomalies are defined as the difference between the target winter and the mean of the preceding five winters, which serves as the reference period. This definition has been shown to be robust to the length of the reference period[19]. The Eurasian domain is defined as the region spanning 40°N–70°N and 0°–140°E, while Northern Europe is defined as 50°N–70°N and 0°–40°E. We also focus on Northern Europe in particular due to the relatively high density of proxy records in this region, as seen in Figure 1, which supports more skillful reconstructions and thus greater confidence in the results. Superposed epoch analysis (SEA)[47] is also used in this study. SEA is a widely used compositing method for isolating the average effect of discrete events, such as volcanic eruptions, from the background variability of the climate system. Statistical significance is assessed using a bootstrap resampling procedure, in which composites from non-volcanic years are drawn 1000 times to establish the 95% confidence level. This threshold is then used as a conservative detection benchmark for assessing whether the temperature anomalies in the first post-eruption winter can be separated from the range of internal variability.

Data availability

The datasets used in this study are publicly available. The HadCRUT5 instrumental temperature dataset is available from the Met Office Hadley Centre at https://www.metoffice.gov.uk/hadobs/hadcrut5/. The WinTEDA reconstruction is available at https://zenodo.org/records/6806314. The ModE-RA reconstruction is available at https://www.wdc-climate.de/ui/entry?acronym=ModE-RA_s14203-18501. The LMR Seasonal dataset is available at https://atmos.uw.edu/~zilumeng/LMR_Seasonal/index.html. The volcanic forcing data used for eruption selection and VSSI values are from the eVolv2k_v3 database, available at https://doi.org/10.26050/WDCC/eVolv2k_v3.

Received: 11 May 2026; Accepted: 25 August 2026;
Published online: 07 September 2026

References

1. LeGrande, A. N. & Anchukaitis, K. J. Volcanic eruptions and climate. *PAGES* **23**, 46–47 https://doi.org/10.22498/pages.23.2.46 (2015).
2. Butchart, N. The brewer-dobson circulation. *Rev. Geophys.* **52**, 157–184 https://doi.org/10.1002/2013RG000448 (2014).
3. Robock, A. Volcanic eruptions and climate. *Rev. Geophys.* **38**, 191–219 https://doi.org/10.1029/1998RG000054 (2000).
4. Groisman, P. Y. Possible regional climate consequences of the Pinatubo eruption: an empirical approach. *Geophys. Res. Lett.* **19**, 1603–1606 https://doi.org/10.1029/92GL01474 (1992).
5. Robock, A. & Mao, J. Winter warming from large volcanic eruptions. *Geophys. Res. Lett.* **19**, 2405–2408 https://doi.org/10.1029/92GL02627 (1992).
6. Robock, A. & Mao, J. The volcanic signal in surface temperature observations. *J. Clim.* **8**, 1086–1103 (1995).
7. Graf, H.-F., Kirchner, I., Robock, A. & Schult, I. Pinatubo eruption winter climate effects: model versus observations. *Clim. Dyn.* **9**, 81–93 https://doi.org/10.1007/BF00210011 (1993).
8. Kodera, K. Influence of volcanic eruptions on the troposphere through stratospheric dynamical processes in the Northern Hemisphere winter. *J. Geophys. Res.: Atmos.* **99**, 1273–1282 https://doi.org/10.1029/93JD02731 (1994).
9. Bittner, M., Schmidt, H., Timmreck, C. & Sienz, F. Using a large ensemble of simulations to assess the Northern Hemisphere stratospheric dynamical response to tropical volcanic eruptions and its uncertainty. *Geophys. Res. Lett.* **43**, 9324–9332 https://doi.org/10.1002/2016GL070587 (2016).
10. Baldwin, M. P. & Dunkerton, T. J. Stratospheric harbingers of anomalous weather regimes. *Science* **294**, 581–584 https://doi.org/10.1126/science.1063315 (2001).
11. Tripathi, O. P., Charlton-Perez, A., Sigmond, M. & Vitart, F. Enhanced long-range forecast skill in boreal winter following stratospheric strong vortex conditions. *Environ. Res. Lett.* **10**, 104007 https://doi.org/10.1088/1748-9326/10/10/104007 (2015).
12. Visbeck, M. H., Hurrell, J. W., Polvani, L. & Cullen, H. M. The North Atlantic Oscillation: past, present, and future. *Proc. Natl. Acad. Sci.* **98**, 12876–12877 https://doi.org/10.1073/pnas.231391598 (2001).
13. Kirchner, I., Stenchikov, G. L., Graf, H.-F., Robock, A. & Antuña, J. C. Climate model simulation of winter warming and summer cooling following the 1991 Mount Pinatubo volcanic eruption. *J. Geophys. Res.: Atmos.* **104**, 19039–19055 https://doi.org/10.1029/1999JD900213 (1999).
14. Thomas, M., Giorgetta, M., Timmreck, C., Graf, H.-F. & Stenchikov, G. Simulation of the climate impact of Mt. Pinatubo eruption using ECHAM5–Part 2: Sensitivity to the phase of the QBO and ENSO. *Atmos. Chem. Phys.* **9**, 3001–3009 https://doi.org/10.5194/acp-9-3001-2009 (2009).
15. Driscoll, S., Bozzo, A., Gray, L. J., Robock, A. & Stenchikov, G. Coupled Model Intercomparison Project 5 (CMIP5) simulations of

climate following volcanic eruptions. *J. Geophys. Res.: Atmos.* **117** https://doi.org/10.1029/2012JD017607 (2012).
16. Toohey, M., Krüger, K., Bittner, M., Timmreck, C. & Schmidt, H. The impact of volcanic aerosol on the Northern Hemisphere stratospheric polar vortex: mechanisms and sensitivity to forcing structure. *Atmos. Chem. Phys.* **14**, 13063–13079 https://doi.org/10.5194/acp-14-13063-2014 (2014).
17. Bittner, M.*On the discrepancy between observed and simulated dynamical responses of Northern Hemisphere winter climate to large tropical volcanic eruptions*. Ph.D. thesis, Universität Hamburg https://doi.org/10.17617/2.2239264 (2015).
18. Polvani, L. M., Banerjee, A. & Schmidt, A. Northern Hemisphere continental winter warming following the 1991 Mt. Pinatubo eruption: reconciling models and observations. *Atmos. Chem. Phys.* **19**, 6351–6366 https://doi.org/10.5194/acp-19-6351-2019 (2019).
19. Polvani, L. M. & Camargo, S. J. Scant evidence for a volcanically forced winter warming over Eurasia following the Krakatau eruption of August 1883. *Atmos. Chem. Phys.* **20**, 13687–13700 https://doi.org/10.5194/acp-20-13687-2020 (2020).
20. Weber, L., Krüger, K. & Fiedler, S. On CMIP6 model consensus for the climate response in Eurasian winter to historical volcanic eruptions. *Geophys. Res. Lett.* **53**, e2025GL120522 https://doi.org/10.1029/2025GL120522 (2026).
21. Zambri, B. & Robock, A. Winter warming and summer monsoon reduction after volcanic eruptions in Coupled Model Intercomparison Project 5 (CMIP5) simulations. *Geophys. Res. Lett.* **43**, 10–920 https://doi.org/10.1002/2016GL070460 (2016).
22. Azoulay, A., Schmidt, H. & Timmreck, C. The Arctic polar vortex response to volcanic forcing of different strengths. *J. Geophys. Res.: Atmos.* **126**, e2020JD034450 https://doi.org/10.1029/2020JD034450 (2021).
23. DallaSanta, K. & Polvani, L. M. Volcanic stratospheric injections up to 160 Tg (S) yield a Eurasian winter warming indistinguishable from internal variability. *Atmos. Chem. Phys.* **22**, 8843–8862 https://doi.org/10.5194/acp-22-8843-2022 (2022).
24. Fischer, E. M. et al. European climate response to tropical volcanic eruptions over the last half millennium. *Geophys. Res. Lett.***34** https://doi.org/10.1029/2006GL027992 (2007).
25. Tejedor, E., Polvani, L. M., Steiger, N. J., Vuille, M. & Smerdon, J. E. No evidence of winter warming in Eurasia following large, low-latitude volcanic eruptions during the Last Millennium. *J. Clim.* **37**, 5653–5673 https://doi.org/10.1175/JCLI-D-23-0625.1 (2024).
26. Steiger, N. J., Smerdon, J. E., Cook, E. R. & Cook, B. I. A reconstruction of global hydroclimate and dynamical variables over the Common Era. *Sci. Data* **5** 1–15, https://doi.org/10.1038/sdata.2018.86 (2018).
27. Hakim, G. J. et al. The last millennium climate reanalysis project: Framework and first results. *J. Geophys. Res.: Atmos.* **121** 6745–6764 https://doi.org/10.1002/2016JD024751 (2016).
28. Tardif, R. et al. Last Millennium Reanalysis with an expanded proxy database and seasonal proxy modeling. *Climate* **15**,1251–1273 (2019).
29. PAGES2k Consortium Continental-scale temperature variability during the past two millennia. *Nat. Geosci.* **6**, 339–346 https://doi.org/10.1038/ngeo1797 (2013).
30. PAGES2k Consortium and others. A global multiproxy database for temperature reconstructions of the Common Era. *Sci. Data* **4** https://doi.org/10.1038/sdata.2017.88 (2017).
31. Meng, Z., Hakim, G. J. & Steig, E. J. Coupled seasonal data assimilation of sea ice, ocean, and atmospheric dynamics over the last millennium. *J. Clim.* **38**, 7229–7247 https://doi.org/10.1175/JCLI-D-25-0048.1 (2025).
32. Perkins, W. & Hakim, G. Coupled atmosphere–ocean reconstruction of the last millennium using online data assimilation. *Paleoceanogr. Paleoclimatol.* **36**, e2020PA003959 https://doi.org/10.1029/2020PA003959 (2021).
33. Penland, C. & Magorian, T. Prediction of Niño 3 sea surface temperatures using linear inverse modeling. *J. Clim.* **6**, 1067–1076 (1993).
34. Valler, V. et al. ModE-RA: a global monthly paleo-reanalysis of the modern era 1421 to 2008. *Sci. Data* **11**, 36 https://doi.org/10.1038/s41597-023-02733-8 (2024).
35. Morice, C. P. et al. An updated assessment of near-surface temperature change from 1850: The HadCRUT5 data set. *J. Geophys. Res.: Atmos.* **126**, e2019JD032361 https://doi.org/10.1029/2019JD032361 (2021).
36. Pauling, A., Luterbacher, J. & Wanner, H. Evaluation of proxies for European and North Atlantic temperature field reconstructions. *Geophys. Res. Lett.* **30** https://doi.org/10.1029/2003GL017589 (2003).
37. Hegerl, G. C., Crowley, T. J., Baum, S. K., Kim, K.-Y. & Hyde, W. T. Detection of volcanic, solar and greenhouse gas signals in paleo-reconstructions of Northern Hemispheric temperature. *Geophys. Res. Lett.* **30** https://doi.org/10.1029/2002GL016635 (2003).
38. Haurwitz, M. W. & Brier, G. W. A critique of the superposed epoch analysis method: its application to solar–weather relations. *Month. Weather Rev.* **109**, 2074–2079 (1981).
39. Sigl, M., Toohey, M., McConnell, J. R., Cole-Dai, J. & Severi, M. Volcanic stratospheric sulfur injections and aerosol optical depth during the Holocene (past 11 500 years) from a bipolar ice-core array. *Earth Syst. Sci. Data* **14**, 3167–3196 https://doi.org/10.5194/essd-14-3167-2022 (2022).
40. Reichen, L. et al. A decade of cold Eurasian winters reconstructed for the early 19th century. *Nat. Commun.* **13**, 2116 https://doi.org/10.1038/s41467-022-29677-8 (2022).
41. Zhu, F. et al. A re-appraisal of the ENSO response to volcanism with paleoclimate data assimilation. *Nat. Commun.* **13**, 747 https://doi.org/10.1038/s41467-022-28210-1 (2022).
42. Toohey, M. et al. Disproportionately strong climate forcing from extratropical explosive volcanic eruptions. *Nat. Geosci.* **12**, 100–107 https://doi.org/10.1038/s41561-018-0286-2 (2019).
43. Burke, A. et al. High sensitivity of summer temperatures to stratospheric sulfur loading from volcanoes in the Northern Hemisphere. *Proc. Natl. Acad. Sci.* **120**, e2221810120 https://doi.org/10.1073/pnas.2221810120 (2023).
44. Yang, L. et al. Persistent stratospheric cold-season aerosols from the 1783 Laki eruption produced winter warming over Northern Eurasia. *Commun. Earth Environ* https://doi.org/10.1038/s43247-026-03197-5 (2026).
45. Evensen, G. The ensemble Kalman filter: theoretical formulation and practical implementation. *Ocean Dyn.* **53**, 343–367 https://doi.org/10.1007/s10236-003-0036-9 (2003).
46. Toohey, M. & Sigl, M. Volcanic stratospheric sulfur injections and aerosol optical depth from 500 BCE to 1900 CE. *Earth Syst. Sci. Data* **9**, 809–831 https://doi.org/10.5194/essd-9-809-2017 (2017).
47. Singh, Y. et al. Statistical considerations in superposed epoch analysis and its applications in space research. *J. Atmos. Sol.-Terr. Phys.* **68**, 803–813 https://doi.org/10.1016/j.jastp.2006.01.007 (2006).

Acknowledgements
This research was supported by NSF Awards 2402475 and 2105805, which supported the research activities reported in this manuscript. We thank Greg Hakim and Eric Steig of the University of Washington for helpful comments and discussions.

Author contributions
Z.M. carried out the data analysis, prepared the figures, and wrote the first draft of the manuscript. L.M.P. contributed to the framing and interpretation

of the results and substantially revised the manuscript. Both authors conceived and designed the study, discussed the results, contributed to the final version of the paper, and approved the submitted manuscript.

Competing interests

The authors declare no competing interests.

Additional information

Supplementary information The online version contains supplementary material available at https://doi.org/10.1038/s41612-026-01535-0.

Correspondence and requests for materials should be addressed to Zilu Meng.